Journal of Ceramic Processing Research. Vol. 20, No. 1, pp. 99~112 (2019)

J O U R N A L O F
Ceramic Processing Research

Effect of yttria on thermal stability, mechanical and in vitro bioactivity properties of hydroxyapatite/alumina composite

Serdar PAZARLIOĞLU* and Serdar SALMAN

Marmara University, Technology Faculty, The Department of Material Science and Engineering, Goztepe Campus, 34722, İstanbul/TURKEY

The phase stability, mechanical and in vitro bioactivity properties of hydroxyapatite/alumina composite with and without yttria were investigated. Hydroxyapatite without additives decomposed at 1300 °C to beta- and alpha-tricalcium phosphate and calcium oxide phases. Although alumina contributed to the mechanical properties of hydroxyapatite, it not only decreased the decomposition temperature of hydroxyapatite from 1200 °C to 900 °C and it's in vitro bioactivity property but also increased the decomposition ratio of hydroxyapatite. An improvement in the properties of hydroxyapatite/alumina composite was provided by yttria via inhibiting the solid-state reactions between hydroxyapatite and alumina via the formation of yttrium aluminum oxide and calcium yttrium trialuminum oxide phases. The maximum fracture toughness of 2.178 ± 0.251 MPam$^{1/2}$, microhardness of 4.947 ± 0.191 GPa, a compressive strength of 227.75 ± 27.87 MPa, and a three-point bending strength of 90.15 ± 6.93 MPa were achieved for hydroxyapatite/alumina composite containing 1.5 wt% yttria at the sintering temperature of 1200 °C. The relative density of 92.94 ± 0.11% was also attained. This ternary composite can potentially be used in the human body for load-bearing applications because of its sufficient mechanical and in vitro bioactivity properties with a decomposition ratio of 9.4%.

Key words: Hydroxyapatite, Alumina, Yttria, Sintering.

Introduction

Hydroxyapatite (HA), is a calcium-phosphate-based bioceramic having a similar composition to bones and teeth. HA, which has exceptional biocompatibility, osteoconductivity, and osteoinductivity, is extensively used in replacement of bones, tissue engineering, drug carriers, and biosensor applications [1]. Even so, usage of HA is still limited due to its low strength and brittle characteristic [2]. To resolve this issue, different approaches have been adopted to improve the mechanical properties of HA, such as adding dopants, making composites with ceramics, and controlling microstructures via novel consolidation techniques [3].

Alumina (Al_2O_3) is a typical engineering ceramic which has high hardness, low friction coefficient, and reduced wear. Al_2O_3 is suitable for structural, automotive, aerospace, biomedical and ballistic applications as well as for cutting tools [4,5]. Previous studies have shown that the mechanical properties of HA can be improved by the addition of Al_2O_3 [6-8]. However, the addition of Al_2O_3 at a high loading to HA not only decreased the decomposition temperature of HA but also facilitated the formation of secondary phases, such as beta-tricalcium phosphate (β-TCP), alpha-tricalcium phosphate (α-TCP), tetra tricalcium phosphate (TTCP) and calcium oxide (CaO). Among them, β-TCP is only usable for temporary applications in the human body because it is resorbable. α-TCP is not suitable for the human body, because its resorbable ratio is higher than the resorbable ratios of both HA and β-TCP. Moreover, CaO is reported to be harmful when used as an implant because of its high reactivity against water. Besides, the existence of CaO could cause the decohesion of implant material, because the formation of $Ca(OH)_2$, and related volume changes could result in internal stresses [9-15]. To eliminate these problems, Al_2O_3 should be added at low loading to HA. Another approach is the addition of an extra material to inhibit the decomposition of HA in HA-Al_2O_3 composites [16].

Yttria (Y_2O_3) has a high melting point of 2462 ± 19°C, and it is satisfied in high-temperature applications [17]. Besides, Y_2O_3 can be used as an additive material without deteriorating the bioactivity of HA because its mechanical properties are higher than that of HA [18,19]. To date, limited investigations on HA-Al_2O_3-Y_2O_3 ternary composites are reported. K.E. Öksüz and A. Özer studied on the microstructural properties of HA-Al_2O_3-Y_2O_3 ternary composites, which consisted of HA-50%Al_2O_3 composited with 0.5% and 1% Y_2O_3 [20]. It was reported by Ref [20] that HA completely decomposed to TCP at a sintering temperature of 1550 °C. No detailed investigations, however, were

*Corresponding author:
Tel : +90(216)-336-57-70 / 1364
Fax: +90(216)-337-89-87
E-mail: spazarlioglu@marmara.edu.tr

reported on the mechanical and in vitro bioactivity properties of HA-Al_2O_3-Y_2O_3 ternary composites.

In the present study, the ternary composites of HA-Al_2O_3-Y_2O_3 were prepared by adding Al_2O_3 and Y_2O_3 at low loadings to avoid decomposition of HA. A series of tests were used to examine the microstructures as well as mechanical and bioactivity properties of HA-Al_2O_3-Y_2O_3 composites.

Experimental Procedure

HA (Across Organics Company, Belgium), Al_2O_3 (Sigma Aldrich, Germany) and Y_2O_3 (Sigma Aldrich, Germany) powders were used as starting materials in the present study. The starting materials were mixed at 180 rpm for 2 h in a zirconia-coated stainless steel with the addition of ethanol and zirconia balls having a diameter of 10 mm to prepare the composites as shown in Table 1. Mixed powders were dried in an oven at 105 ºC for 1 d. Subsequently, 1.810 g powders were pressed into pellets under 350 MPa according to British 7253 standard [22]. Pelleted samples were sintered for 4 h at five temperatures ranging from 900 ºC and 1300 ºC. The ramp rate was 5 ºCmin^{-1}. Phase analysis using a Philips X'Pert X-ray diffraction (XRD, Netherlands) device was performed to the powders obtained from compression test samples which were crushed in a ceramic mortar. Cu-Kα was used as the radiation source at a scan speed of 0.6 º min^{-1} and a step scan of 0.02 º in the range of 2θ values between 25 º and 50 º. The decomposition ratio of sintered samples was determined by Rietvield analysis based on the results of the XRD analysis. The surface morphology of the sintered samples was determined using FEI Sirion XL30 scanning electron microscope (SEM, USA) after gold sputtering. The variations in the average grain size were determined by the lineal intercept method.

Table 1. Chemical composition of HA powder used as matrix material in the present study.

Base elements	Type of impurity	ASTM F1185-88 (ppm)	HA (ppm)
Ca (39.894) P (18.498)			
	As	3	≤2
	Hg	5	≤1
	Pb	30	≤5
	Cd	5	≤2
	Total of heavy metals	50	≤10
	Cl		≤1500
	Cu		≤20
	F		≤50
	Fe		≤400
	Mn		≤20
	SO_4^{2-}		≤5000

Table 2. The compositions of the samples

Group		Composition (wt%)
1		HA (%100)
2		HA-5Al_2O_3
3	3.1	HA-5Al_2O_3-0.5Y_2O_3
	3.2	HA-5Al_2O_3-1.5 Y_2O_3
	3.3	HA-5Al_2O_3-2.5 Y_2O_3

Green densities of the pelleted samples were calculated by dividing mass against volume. Apperant densities and porosities of the sintered samples were calculated using Archimedes method. Theoretical densities of the samples were calculated as 3.156, 3.188, 3.194, 3.206, and 3.218 g.cm^{-3} for monolithic HA, HA-5A and HA-5A-05.Y, 1.5Y and 2.5Y composites, respectively, according to mixture rule. Theoretical densities the raw materials were separately taken as 3.156 g.cm^{-3} for HA [23], 3.970 g.cm^{-3} for Al_2O_3 [24] and 5.032 g.cm^{-3} for Y_2O_3 [25], respectively. To calculate the shortening percentage of sintered samples, the lengths of each sample before and after the sintering process were compared using an electronic caliper having a sensitivity of 1/1000. The samples were firstly ground using 800, 1200, and 2500 mesh SiC papers and then polished with 10, 5, 3, and 1 μm diamond pastes until mirror-like surfaces were achieved for microhardness and fracture toughness measurements. 200 g load for 20 s was applied for microhardness measurements, and 300 g load for 10 s was used for fracture toughness measurements. To calculate the average values and standard deviations, 10 indentations were taken from the surfaces of three samples for both tests. Fracture toughness values were calculated using Niihara equation [26]. Compression tests were carried out on 10 samples using a universal testing machine (Devotrans FU 50kN, Turkey) under a loading rate of 2 mm.min^{-1}. Three-point bending strength ($\sigma_{T.P.B.}$) strength measurements were carried to 5 different performed on five samples, which were prepared according to ASTM C1161-94 standard [27] at a cross head speed of 1 mm.min^{-1} until broken. The inner and outer support rings had diameters of 10 and 20 mm, respectively. The gap between inner spans was 20 mm. The sintered test bars were ground (1200 grit) on both sides before testing. The in vitro bioactivity properties of the monolithic HA, HA-5A, and HA-5A-1.5Y ternary composites were determined by simulated body fluid (SBF) prepared according to Ref [28]. Before the in vitro tests, four samples were sintered to temperatures at which the highest compressive strength values were attained for a size of Ø11 and 4 mm^2. After this stage, the samples were ground by 400, 600, 800, 1000, and 1200 mesh SiC papers before being dried in an oven at 105 ºC for 1 d. The samples were immersed in sealed test tubes containing 20 mL of SBF solutions for 3, 7, 15, and 30 d. The 20 mL SBF solutions used in the in

vitro tests were changed every day. At a specified time, the samples were taken from the SBF solutions without damaging the apatite layers and cleaned using distilled water. Finally, the samples were dried at 60 °C for 12 h. The apatite layers on the surface of samples immersed in SBF solutions were investigated by SEM.

Results and Discussion

Microstructural properties

Fig 1 and Fig 2 illustrate the SEM images and average grain sizes of the starting materials, respectively. HA had evidently agglomerated particulates were in irregular shapes and an average grain size of 7.096 μm. Al_2O_3 presented an alpha structure with irregular shapes and an average grain size of 8.334 μm. Y_2O_3 also possessed irregular shapes and an average grain size of 7.408 μm.

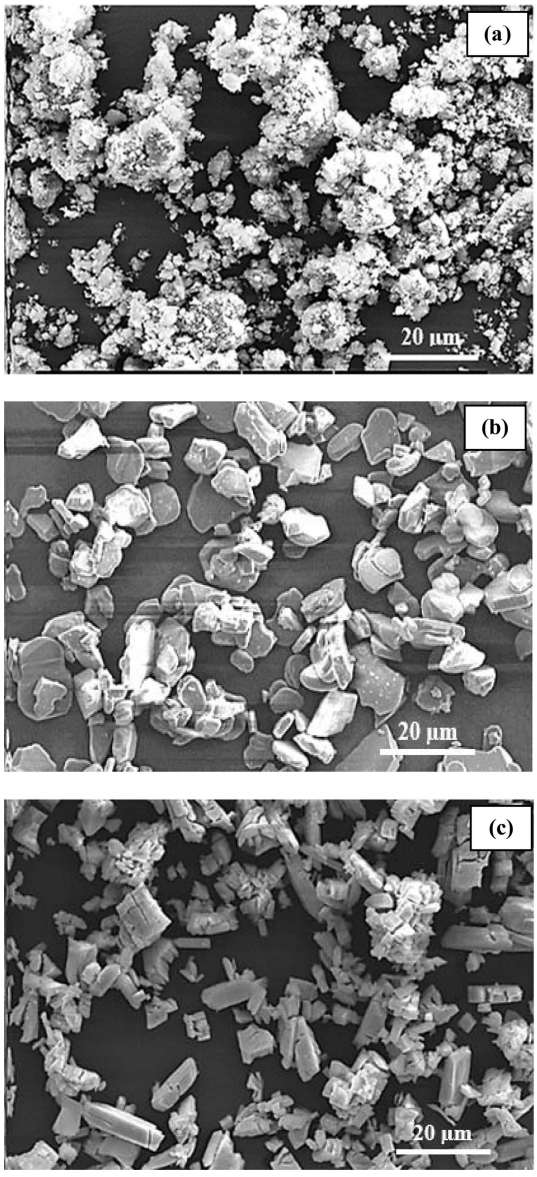

Fig. 1. SEM image of (a) HA, (b) Al_2O_3 and (c) Y_2O_3 powder.

These results indicate that three types of powders had similar median particle sizes. Fig. 3 shows the XRD patterns of starting materials. The HA powder used in the present study consisted of HA peaks compatible with XRD card number of 98-008-0526. According to the chemical composition (Table 1) given by Across Organics Company, HA can be used in biomedical applications because it agreed with ASTM F1185-88 standard [21].

Fig 4 shows the XRD patterns of HA without additives sintered at specified temperatures. Monolithic HA consisted of HA peaks until the sintering temperature reached to 1100 °C. Sintering at 1200 °C caused the decomposition of HA, which was determined by the presence of β-TCP (an XRD card number of 98-007-6896) in addition to HA peaks. At 1300 °C, decomposition was still observed because α-TCP (an XRD card number of 98-007-8499) and CaO (an XRD card number of 98-003-4977) phases were detected in addition to the HA and β-TCP. The decomposition of pure HA at the sintering temperature of 1300 °C can be explained by Reaction 3.1 [29]. ($Ca_3(PO4)_2$ is β-TCP, and $Ca_3P_2O_8$ iss α-TCP)

$$Ca_{10}(PO_4)_6(OH)_2 \longrightarrow 2Ca_3(PO4)_2 + Ca_3P_2O_8 + CaO + H_2O \quad (3.1)$$

Although HA decomposed at temperatures which

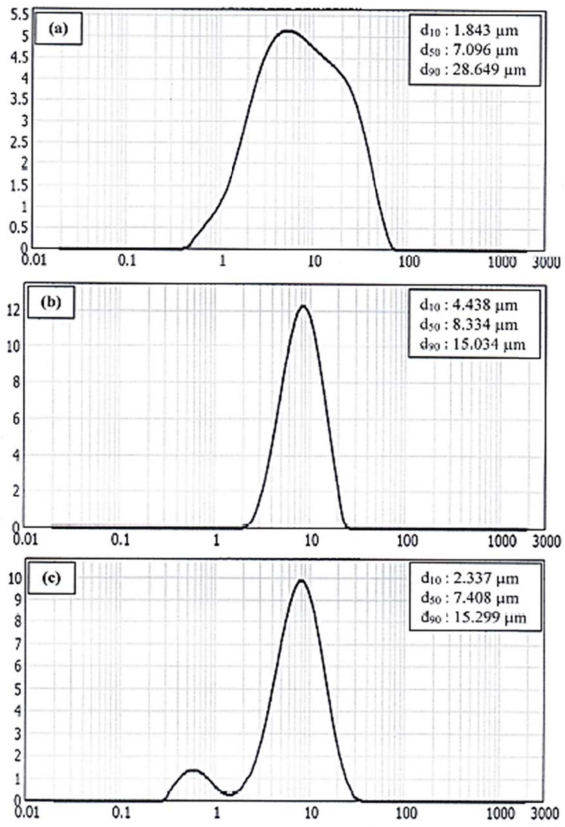

Fig. 2. Particulate size of (a) HA, (b) Al_2O_3 and (c) Y_2O_3 powder.

were higher than 1100 °C, the main phase was still HA at all sintering temperatures. HA-Al_2O_3 composite included the peaks of α-Al_2O_3 and calcium aluminates such as $Ca_3Al_2O_6$, $CaAl_4O_7$, and $CaAl_2O_4$ in addition to HA, β-TCP, and α-TCP as shown in Fig 5. It was determined that α-Al_2O_3 phase was found at all sintering temperatures. The $Ca_3Al_2O_6$ and $CaAl_4O_7$ phases remained up to 1100 °C and 1200 °C, respectively. $CaAl_2O_4$ appeared at the sintering temperatures of 1200 °C and 1300 °C. As stated in previous reports [30-32], these calcium aluminates have positive effects on the improvement of bioactivity of some materials used in the human body. Calcium aluminates are formed due to the solid-state reactions between HA and Al_2O_3 powders [33]. Fig. 5 also revealed that the addition of Al_2O_3 to HA reduced the decomposition temperature of HA from 1200 °C to 900 °C. Solid-state reactions in ionic materials occur by the diffusion of ions across the interface. In the present case, for the formation of calcium aluminates, Ca^{2+} and Al^{3+} are important species. The reaction can take place in two ways, i.e., Al^{3+} can diffuse into HA, or Ca^{2+} can diffuse from the HA into Al_2O_3 [16]. Fig. 6 shows the XRD analysis of Y_2O_3 added composites. Y^{+3}-containing phases, such as yttrium aluminum oxide ($AlYO_3$, XRD card number of 98-000-1802), calcium yttrium trialuminum oxide ($CaAl_3YO_7$, XRD card number of 98-001-6827), and Y_2O_3 (XRD card number of 98-003-4446), were detected in addition to HA, β-TCP, α-TCP, and calcium aluminate phases. While $AlYO_3$ and Y_2O_3 were detected to HA-5A-Y composites at all sintering temperatures, $CaAl_3Y_7$ phase was only observed for HA-5A-2.5Y at all sintering temperatures. The CaO phase was not detected for pure HA. This was because of the usage of Al_2O_3 at low loadings and formation of $AlYO_3$ and $CaAl_3YO_7$ phases, which could inhibit the reaction between HA and Al_2O_3. The $AlYO_3$ has an orthorhombic crystal lattice structure with a = 5.330 Å, b = 7.375 Å and c = 5.180 Å as well as with α = 90 °, β = 90 ° and γ = α = 90 ° [34], which occurs at the interface of Al_2O_3 and Y_2O_3 powders as reported in previous reports [35,36] according to Reaction 3.2.

$$Y_2O_3 + Al_2O_3 \longrightarrow 2AlYO_3 \quad (3.2)$$

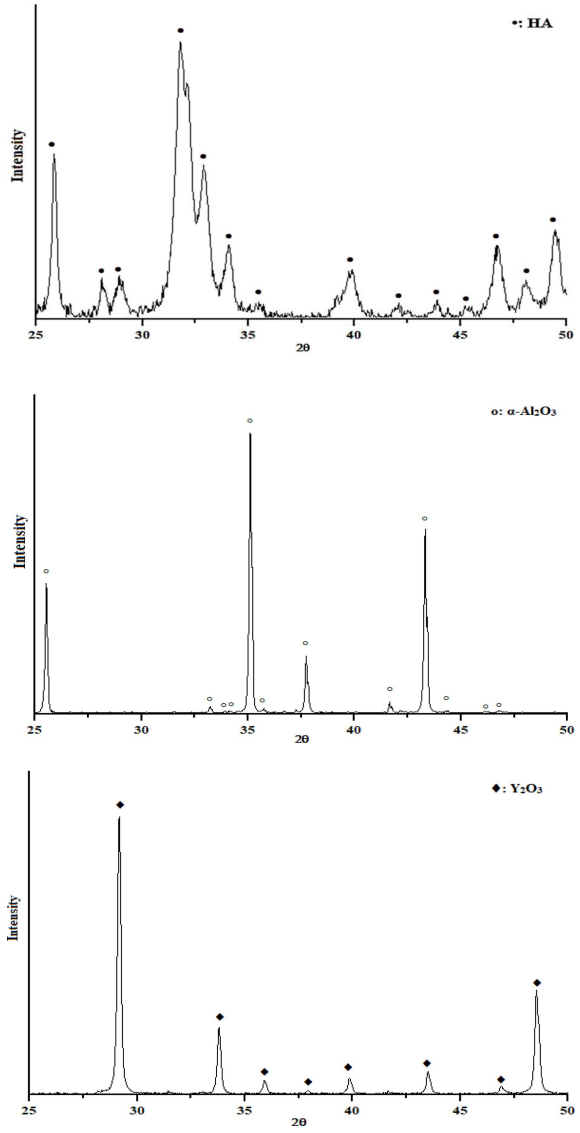

Fig. 3. XRD analysis of starting powders at room temperature.

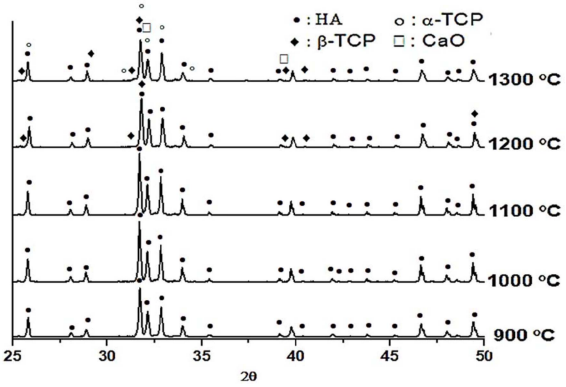

Fig 4 XRD analysis of HA without additives depending sintering temperatures.

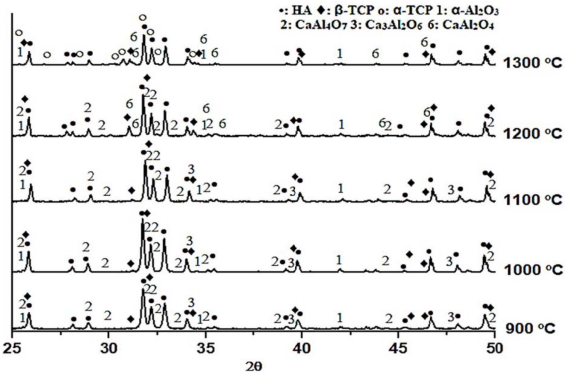

Fig. 5. XRD analysis of HA-5A binary composites depending on the sintering temperatures.

Table 3. Rietveld analysis of monolithic HA.

Sample	Phases	Sintering temperature (°C)				
		900	1000	1100	1200	1300
HA	HA	100	100	100	96.2	94.2
	β-TCP	-	-	-	3.8	4.1
	α-TCP	-	-	-	-	1.6
	CaO	-	-	-	-	0.1

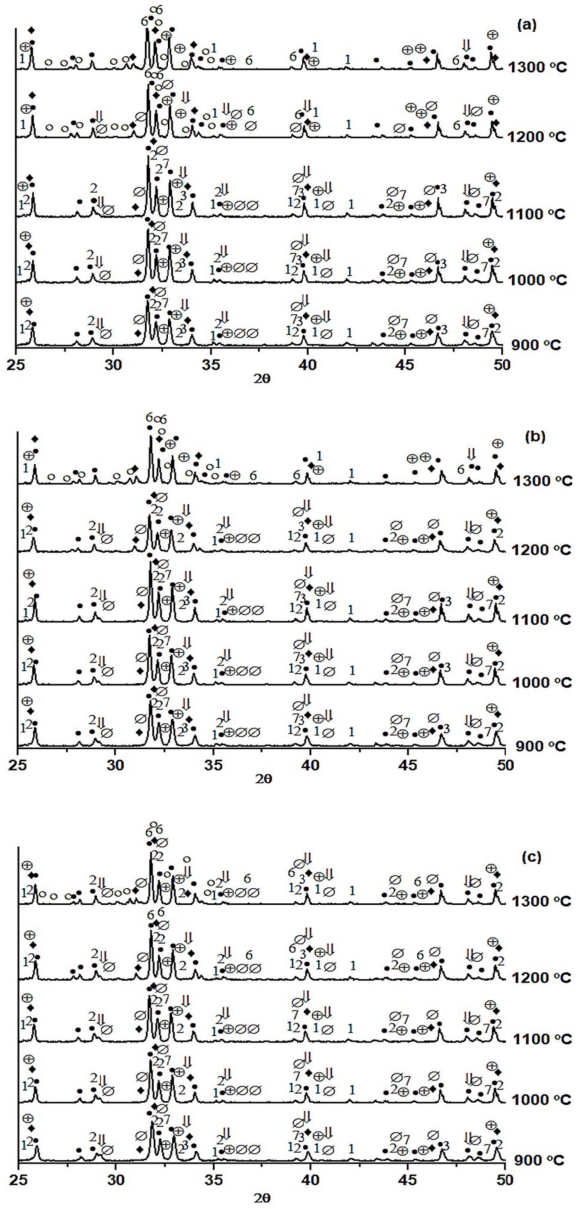

Fig. 6. XRD analysis of (a) HA-5A-0.5Y, (b) HA-5A-1.5Y and (c) HA-5A-2.5Y ternary composites depending on sintering temperatures (•: HA, ♦: β-TCP, ○: α-TCP, 1: α-Al_2O_3, 2: $CaAl_4O_7$, 3: $Ca_3Al_2O_6$, 6: $CaAl_2O_4$, : $AlYO_3$, : $CaAl_3YO_7$, ⇓ : Y_2O_3)

$CaAl_3YO_7$ has a tetragonal crystal lattice structure with lattice parameters of a = 7.676 Å, b = 7.676 Å and c = 5.040 Å as well as with α = 90 °, β = 90°, γ = 90 °.

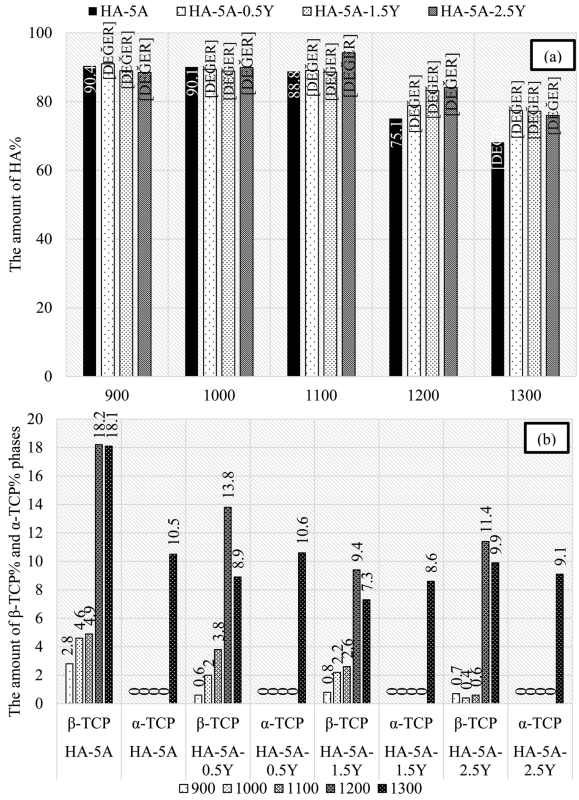

Fig. 7. Relative amount of HA decomposed to TCP in HA with additives depending on the sintering temperatures.

Morever, it has been also detected in the CaO-Al_2O_3-Y_2O_3 ternary phase diagram as reported by Ref [37]. The formation of Y^{3+}-containing phases is not only related to the ion radius of Y^{3+} (0.93 Å [38]), Al^{3+} (0.51 Å [39]), and Ca^{2+} (0.99 Å [40]) but also related to the close distance between Y-O (2.366 Å [41]) and Ca-O (2.380 Å [42]).

Table 3 shows the Rietveld analysis of pure HA. The amount of secondary phases in pure HA was less than 5%, and the main phase was HA at all sintering temperatures. Fig. 7 shows the Rietveld analysis of HA-5A binary composite with and without Y_2O_3. The amount of HA% in HA-5A binary composite decreased from 90.4% to 68.2% by increasing sintering temperatures. The decomposition rate of HA-5A composite agreed with a previous report [43]. Fig. 7(a) reveals that the amount of HA% in HA-5A composites can be increased by Y_2O_3 additive at all sintering temperatures. The HA% in HA-5A-0.5Y, HA-5A-1.5Y, and HA-5A-2.5Y composites decreased from 91% to 77.4%, from 89% to 77.2%, and from 88.5% to 76%, respectively. The amount of β-TCP was about 18% for HA-5A composite at elevated temperatures. Via compositing with 1.5% Y_2O_3, the reduction was about 50%-60% at the amount of β-TCP in HA-5A composite, when sintering had performed at the temperatures of 1200 °C and 1300 °C, respectively. Although the additions of Y_2O_3 at 0.5% and 2.5% reduced the β-TCP

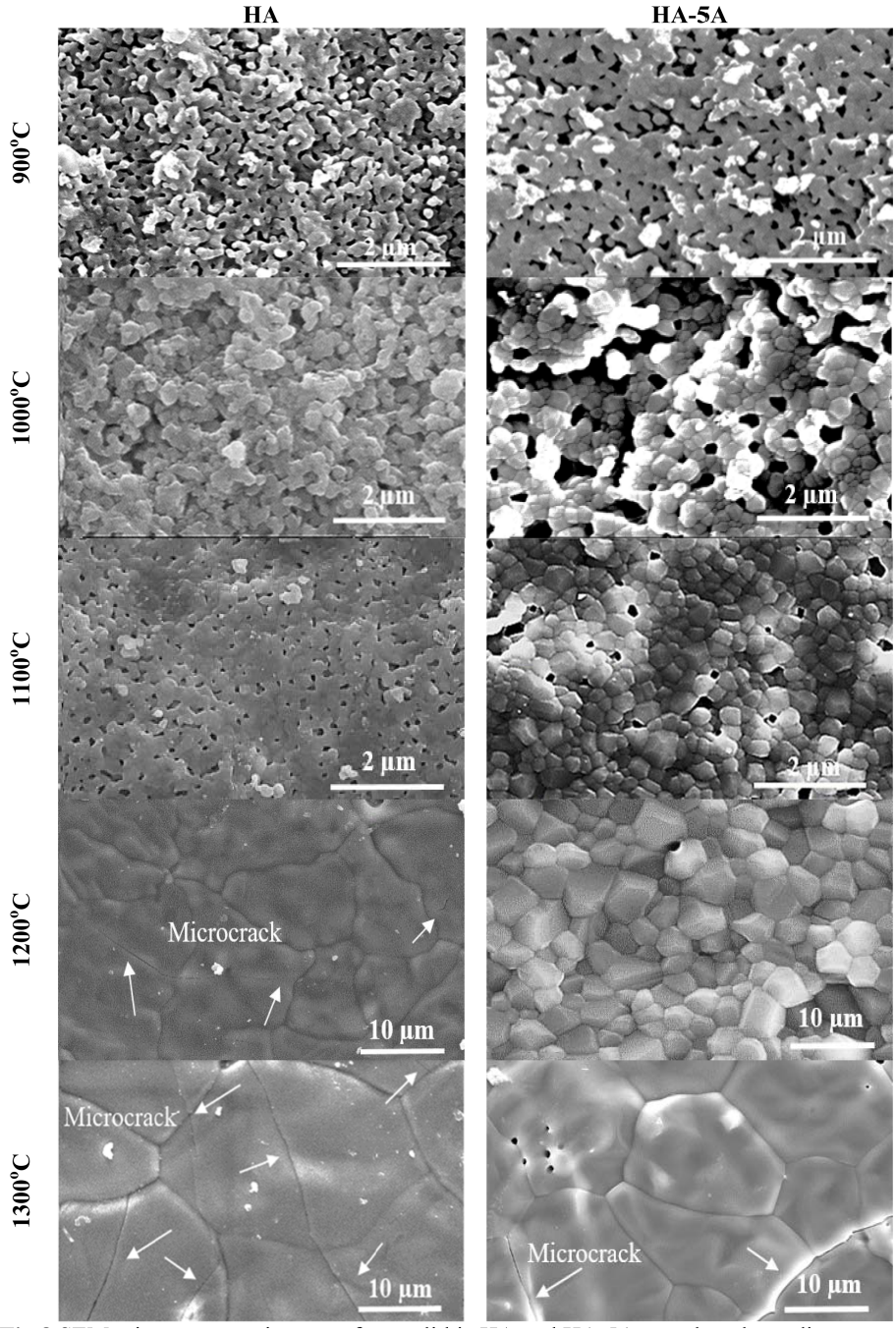

Fig. 8. SEM microstructure images of monolithic HA and HA-5A samples, depending on the sintering temperatures.

ratios of HA-5A composite, the highest reduction rates were achieved by adding 1.5% Y_2O_3. α-TCP appeared only at sintering temperature of 1300 ºC, in the present study. The ratio of α-TCP of the HA-5A binary composite at this temperature increased only in the ternary composite of HA-5A-0.5Y at a negligible level, but it was in low rates to the others.

As far as the decomposition rates of the HA-5A-Y ternary composites were concerned, it was determined that the HA-5A-1.5Y ternary composite decomposed at lower rates than the others. The ternary composites formed by adding Y_2O_3 in this study had a high stability at elevated temperatures, compared to previous studies [44-47]. Such a result is related to the low reactivity characteristics of the added powders to HA.

Fig. 8 and Fig. 9 show the SEM images of HA with and without additives. The following results can be revealed: i) Sintered samples between 900 ºC and 1100 ºC were porous. ii) An excessive grain growth occurred in monolithic HA at elevated temperatures, which could be minimized by additives. iii) Microcracks were observed on the surface of samples after sintering

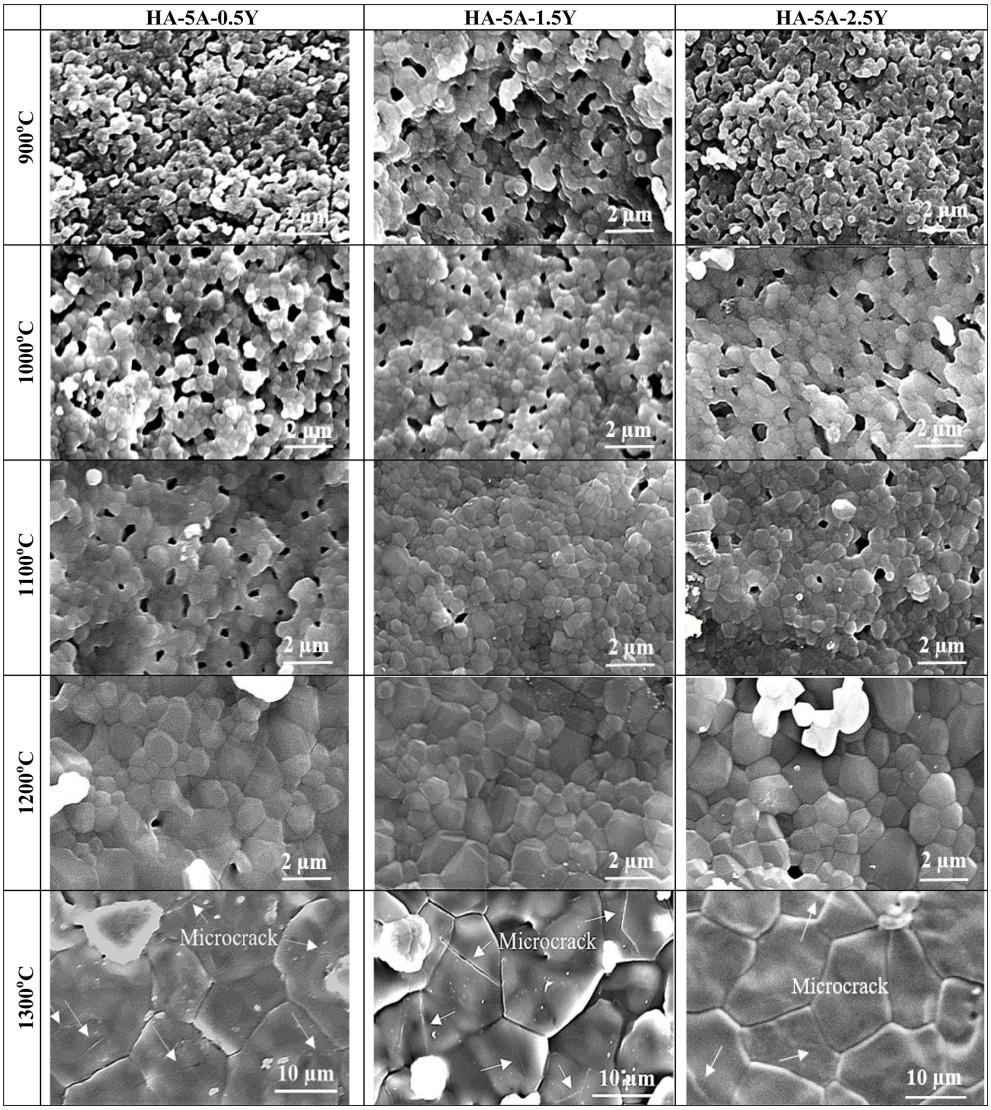

Fig. 9. SEM microstructure images of Y_2O_3 added samples depending on sintering temperatures.

at elevated temperatures. iv) Addition of Y_2O_3 to the HA-5A composite contributed to the formation of homogenous microstructures. Porous structures are related to the insufficient sinterability of samples. Grain growth of HA at elevated temperatures could be decreased by additives because their thermal expansion coefficient (TEC) was lower than that of HA. The TEC values of HA, Al_2O_3, and Y_2O_3 are 13.6×10^{-6} [48], 8×10^{o6} [49] and 8.9×10^{-6} [50] as stated in previous literatures. The low TEC of additive materials contribute the improvement of the mechanical properties of monolithic HA as declerated by Ref [51]. It has been well established that a decrease in grain size increased the mechanical properties according to the Hall-Petch equation ($\sigma = \sigma_o + kd^{-1/2}$) [52]. Microcracks observed at elevated temperatures are related to the presence of β- and α-TCP phases. It has been well described in previous studies that β- and α-TCP phases have the different TEC values than that of HA [53]. Microcracks, which was imaged on the surface of monolithic HA sintered at elevated temperatures, had a transgranular morphology as in HA-5A and HA-5A-Y composites, but they presented bigger sizes compared to samples composited with Al_2O_3 and Y_2O_3. This could be explained by the average grain sizes of the sintered samples, as shown in Fig. 10. The average grain sizes of pure HA were determined to be 0.162 ± 0.019 μm at 900 °C, 0.186 ± 0.020 μm at 1000 °C, 0.473 ± 0.035 μm at 1100 °C, 7.955 ± 1.166 μm at 1200 °C and 17.167 ± 2.156 μm at 1300 °C. The grain sizes of HA-5A composite were 0.109 ± 0.014, 0.199 ± 0.019, 0.427 ± 0.033, 0.812 ± 0.110, and 10.171 ± 3.157 μm. The average grain size of HA-5A composite sintered at 1200 °C and 1300 °C were about 88% and 40% of pure HA. The samples composited with Y_2O_3 had 90% and 50% average grain sizes of pure HA. As shown in these values, addition of Y_2O_3 enabled us to prevent excessive grain growth of pure HA as well as HA-5A composite,

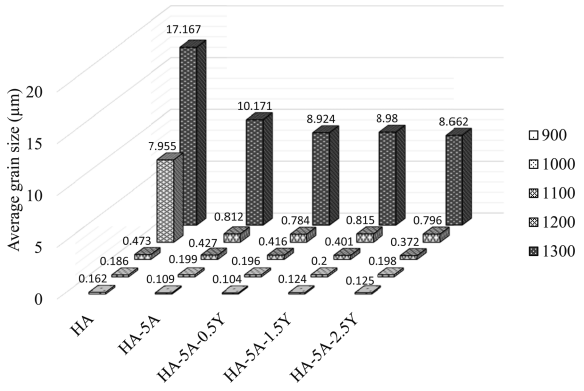

Fig. 10. Average grain size of the samples.

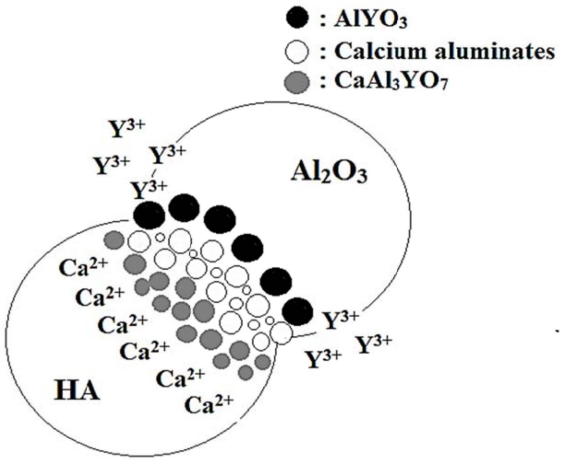

Fig. 11. Schematic representation of the inhibition of solid-state reactions between HA and Al_2O_3 powders with Y_2O_3 additive**.**

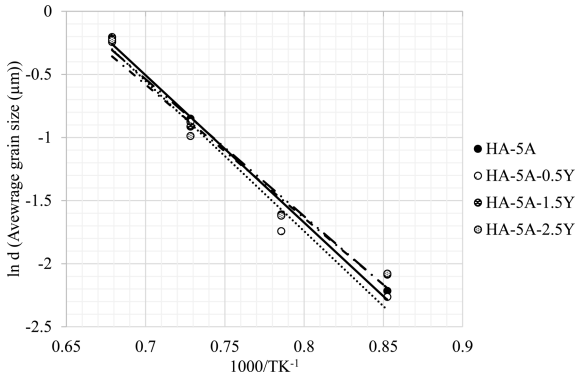

Fig. 12. Activation energy curves of the samples.

which can be related to the presence of $AlYO_3$ and $CaAl_3YO_7$ phases. Low grain sizes led to a high barrier for the progression of microcracks. Via the formation of $AlYO_3$ and $CaAl_3YO_7$ phases, the amount of β- and α-TCP phases could be minimized. In the other words, decomposition was successfully hindered because of the inhibition of the solid-state reactions between HA and Al_2O_3 powders as shown in Fig. 11.

Fig. 12 shows the activation energy for grain growth of samples. The activation energy value of pure HA was determined to be 178.83 kJ mol^{-1} (42.56 kcal mol^{-1}). As stated by P. Layrolle [54], the activation energy of HA ranges from 120 to 240 kJ mol^{-1} (28.6- 57.3 kcal mol^{-1}). The activation energy of HA-5A composite was found to be 173.95 kJ mol^{-1} (41.40 kcal mol^{-1}). HA-5A composite has lower activation energy than that of HA because of the inhibition of the growth of HA grains due to the presence of calcium aluminate phases, which were detected by XRD analysis. The activation energies of HA-5A-0.5Y, HA-5A-1.5Y, and HA-5A-2.5Y composites were calculated as 169.60, 164.23, and 163.68 kJ mol^{-1}, respectively. These values indicated that the activation energies of samples composited with Y_2O_3 were lower than that of monolithic HA, which is about 7%. As stated by Ref [55, 56] that a high level of activation energy needed to reach large grain sizes.

Physical and mechanical properties

Fig. 13 illustrates the physical properties of sintered samples. With increasing sintering temperature, the shrinkage and density increased, and the porosity decreased as expected. The maximum shrinkage (18.20 ± 0.62%) was obtained for pure HA at the sintering temperature of 1300 ºC. At this maximum shrinkage, the pure HA reached a density of 3.064 ± 0.024 g cm^{-3} and a relative density of 98.353 ± 0.176%. with a porosity of 2.912 ± 0.769%.

The shrinkage rate as well as other properties of composites were generally lower than that of pure HA. Without Y_2O_3, the maximum shrinkage of the HA-5A composite was 17.263 ± 0.751%, which could be improved by adding Y_2O_3 at about 2%. Although the addition of Y_2O_3 increased the shortening rate of HA-5A composite, the other physical properties of HA-5A-Y ternary composites were lower than that of both HA-5A and pure HA. The same situation was also observed for HA-based bioceramics which included two different oxide ceramics as an additive material, such as ZrO_2-La_2O_3 [57] and MgO-ZrO_2 [58]. The sintered density of the composites were lower than that of pure HA for two reasons: First, the decrease in average grain size by additives, which led to the formation of porous structures. Second, the amount of β- and α-TCP of the composites, which have lower theoretical density values compared to HA, were higher than that of HA (HA: 3.156 g cm^{-3}, β-TCP: 3.07 g cm^{-3} [59], and α-TCP: 2.86 g cm^{-3} [60]). As could be seen from the SEM images, porous structures had generated because of low levels of neck formation among grains for sintered samples up to 1100 ºC. After sintering at 1200 ºC, the densification rates of the samples increased sharply and reached the maximum values, which varied between 90% and 92% for HA with additives. At those densification rates, the mechanical properties of the composites also presented the maximum values as shown in Fig. 14. Densification at around 90% is

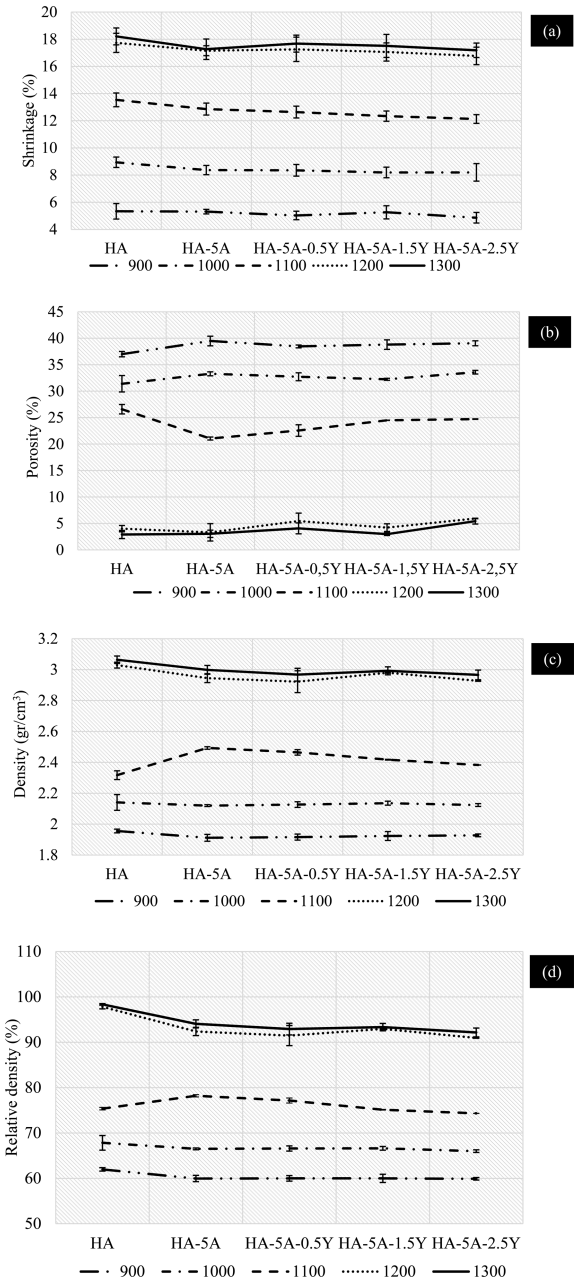

Fig. 13. Physical properties of sintered samples.

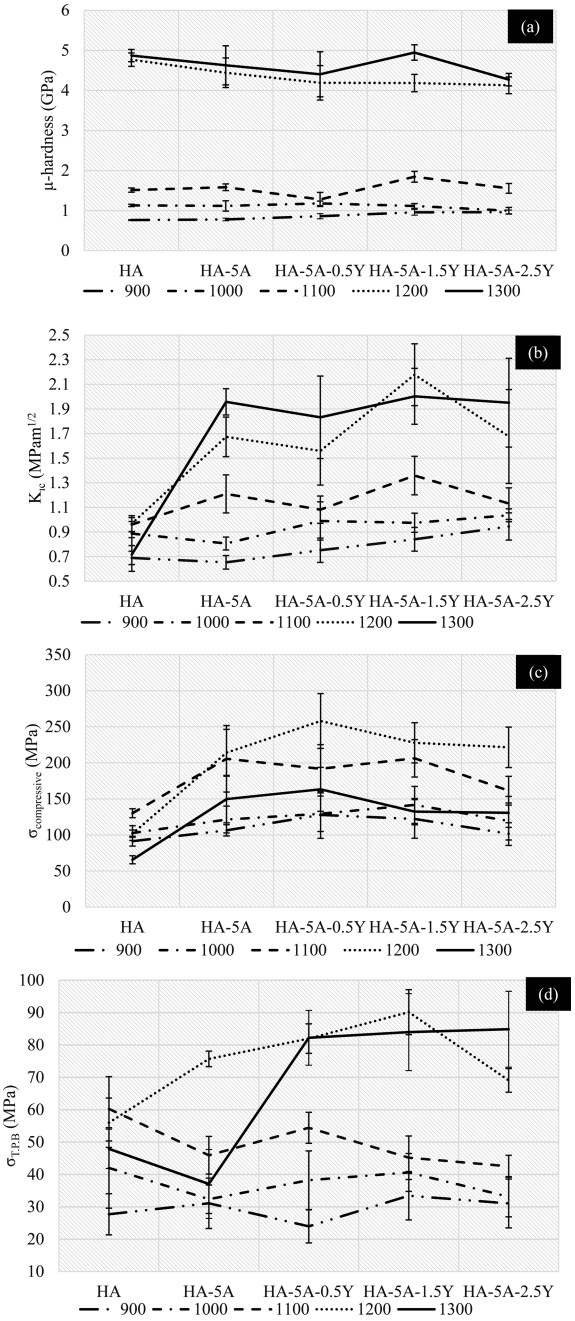

Fig. 14. Mechanical properties of the sintered samples.

desirable because of the presence of a certain degree of porosity as well as of reabsorbable phases (α- and β-TCP) contributing to bone intergrowth and a subsequent implant-bone interfacial adhesion [61]. It has been successfully achieved in the present study. Fig. 14 shows the mechanical properties of the samples. Except microhardness, the mechanical properties of monolithic HA reached the maximum values just before densification was completed. The mechanical strength values of pure HA were 0.96 ± 0.05 MPam$^{1/2}$ for Kıc, 130 ± 6.22 MPa for $\sigma_{compressive}$, 60.27 ± 9.93 MPa for $\sigma_{T.P.B.}$, and 4.87 ± 0.15 GPa for microhardness. Even though microhardness increased with increasing densification, the reduction in mechanical properties just before densification of pure HA was also observed previously [62,63]. The increase in density of ceramic materials improved the mechanical properties, however; HA which was sintered at temperatures of 1250-1300 ºC decomposed and formed inhomogeneous grains with low mechanical properties [64–66]. Increment in microhardness value was related to the fact that the β-TCP phase increased the hardness of monolithic HA ceramics as stated by a previous report [67]. The highest microhardness value was 4.62 ± 0.48 GPa for the HA-5A composite, and it was 4.40 ± 0.56, 4.95 ± 0.19, and 4.27 ± 0.15 GPa for HA-5A-Y ternary composites. Although the amount of β-TCP in HA with additives was higher than that of pure HA,

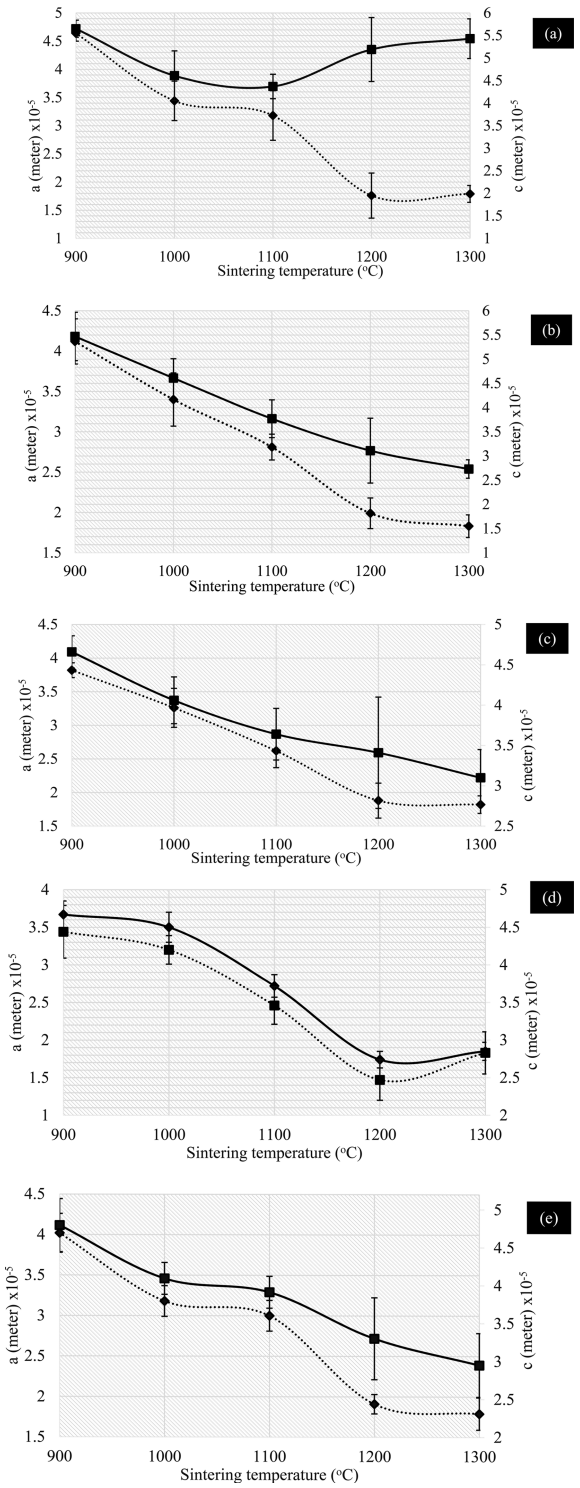

Fig. 15. a and c values of measured at Kıc test of (a) monolithic HA, (b) HA-5A, (c) HA-5A-0.5Y, (d) HA-5A-1.5Y and (e) HA-5A-2.5Y samples depending on sintering temperatures.

their microhardness was generally lower than that of HA because of porous structures. Low fracture toughness of HA restricts its load-bearing applications in the human body. Fracture toughness of HA varies nonmonotonically with grain size. It reaches a peak value at a grain size of about 0.4 μm [68], and changes between 0.8 and 1.2 $MPam^{1/2}$ [69]. In the present study, the $K_{ıc}$ of pure HA reached the peak value of 0.96 ± 0.05 $MPam^{1/2}$ at an average grain size of 0.473 ± 0.035 μm with a c/a ratio of 1.37 ± 0.05. However, it drastically decreased when the average grain sizes were 7.96 ± 1.17 μm at 1200 °C and 17.17 ± 2.16 μm at 1300 °C. At those temperatures, the reduction rates in $K_{ıc}$ values were 5% and 27%, and the c/a ratios were about 2.94 ± 0.39 and 3.06 ± 0.44, respectively. The size of the microindentation cracks increased as shown in Fig. 15 because of the increased grain size [70]. Low fracture toughness of HA can be improved by increasing the number of grain boundaries via decreasing the growth rate of HA grains, which causes the growth of intergranular cracks instead of the transgranular ones [71].

With increasing temperature, $K_{ıc}$ of HA-5A composites increased to the maximum value of 1.95 ± 0.10 $MPam^{1/2}$, which is approximately two times higher than the peak $K_{ıc}$ value of pure HA. Moreover, the c/a ratio of the HA-5A (1.49 ± 0.10) composite at 1300 °C was about 51% of pure HA ($c/a = 3.06 \pm 0.44$). The calcium aluminate phases formed by the addition of Al_2O_3 resulted in the alteration and bridging of cracks occurring during the decomposition of HA, which strengthened the matrix against the formation of large cracks [72]. Therefore, the fracture toughness values of Al_2O_3-reinforced samples were higher than that of pure HA. Although the $K_{ıc}$ value of the HA-5A composite was compatible with a previous study on HA-Al_2O_3 composite [73], it was lower than that of the Kıc value of human cortical bone (2-6 $MPam^{1/2}$) [74]. It was related to two main reasons: First, the cortical bone is a composite material with an advanced structure consisting of collagen fiber-HAp crystallite networks (epitaxy) at the molecular level, a lamellar structure at the microstructural level, and aligned cylindrical units at the macrostructural level [75]. Second, the fracture toughness and energy of Al_2O_3 are not too high compared to other oxide ceramics such as ZrO_2 [76]. The $K_{ıc}$ values of HA-5A-Y ternary composites increased with increasing Y_2O_3 at 900 °C and 1000 °C. The highest $K_{ıc}$ values of 1.359 ± 0.156, 2.178 ± 0.251, and 2.002 ± 0.227 $MPam^{1/2}$ belonged to HA-5A-1.5Y ternary composites between the sintering temperatures of 1100 °C and 1300 °C. The $K_{ıc}$ values of HA-5A-0.5Y and HA-5A-2.5Y composites increased at 1300 °C as in HA-5A binary composite and reached 1.832 ± 0.334 and 1.951 ± 0.360 $MPam^{1/2}$, respectively. The highest $K_{ıc}$ value of 2.178 ± 0.251 $MPam^{1/2}$ for HA-5A-1.5Y composite sintered at 1200 °C was obtained at an average grain size of 0.815 ± 0.149 with a c/a ratio of 1.415 ± 0.09. At that temperature, although the c/a value of the HA-5A-1.5Y composite was lower than that of pure HA at about 51.87%, the maximum $K_{ıc}$ value was approximately 2.28 times higher than that of pure HA. Moreover, it can be used in the human body for load-bearing

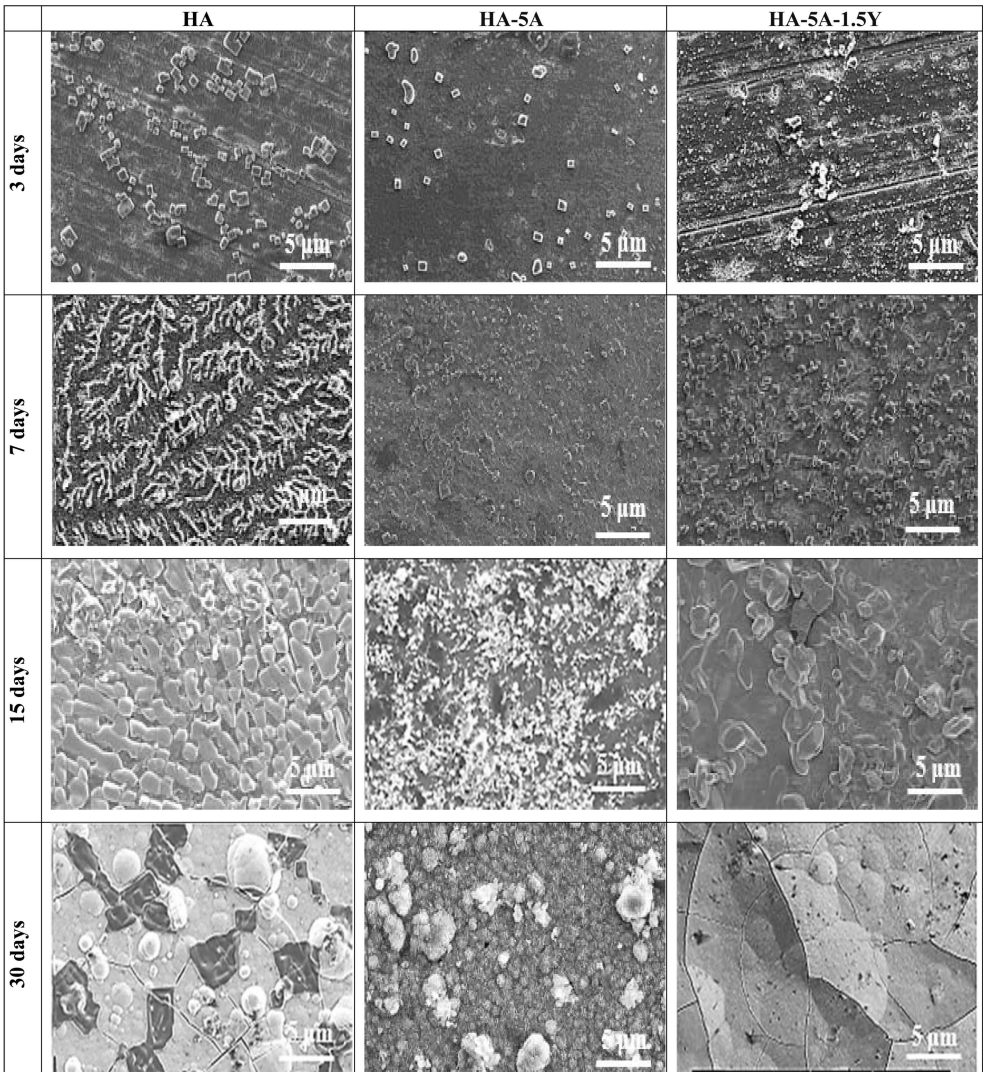

Fig. 16. SEM images of the samples immersed into SBF solution.

applications because the maximum K_{ic} value of 2.178 ± 0.251 $MPam^{1/2}$ was in the range of K_{ic} values of the cortical bone.

Although $\sigma_{compressive}$ of pure HA reached the maximum value of 130 ± 6.22 MPa at the sintering temperature of 1100 °C, $\sigma_{compressive}$ of the composites presented the maximum values at 1200 °C. At temperatures above 1100 °C, $\sigma_{compressive}$ values of pure HA were calculated as 101.8 ± 5.01 and 65.6 ± 5.59 MPa, respectively. The sample with 5 wt% Al_2O_3 possessed $\sigma_{compressive}$ of 214 ± 32.50 MPa, which was higher than the maximum $\sigma_{compressive}$ of pure HA. This maximum $\sigma_{compressive}$ of HA-5A was comparable with a previous study in which HA was doped by 15 wt% Al_2O_3 [77].

However, $\sigma_{compressive}$ of the HA-5A sample sintered at 1300 °C (149.7 ± 32.8 MPa) was 69% of HA-5A sintered at 1200 °C. Such a reduction could be attributed to the α-TCP and $CaAl_2O_4$ phases. A decrease in $\sigma_{compressive}$ values was also observed for Y_2O_3 added samples which had sintered at the temperature of 1300 °C. As reported by Ref [78, 79] that $CaAl_2O_4$ is a phase formed in HA-Al_2O_3 system, which accelerate the decomposition of HA into α-TCP phase. TCP is available in two forms of β-TCP and α-TCP. β-TCP has a hexagonal crystal lattice structure of type R3CH and unit cell dimensions of a = b = 10.439 Å and c = 37.375 Å as well as with α = β = 90 ° and γ = 120 ° [80], and its compressive strength is about 120 MPa [81]. α-TCP has a monoclinic crystal lattice structure of P21/a type and has unit cell dimensions of a = 12.859 Å, b = 27.354 Å, and c = 15.222 Å, and α = 90°, β = 126.35 °, and γ = 90 °. Its compressive strength is about 10 to 30 MPa [82, 83]. $\sigma_{compressive}$ of the samples sintered at 1300 °C decreased not only because of microcracking arising from the combined expansions associated with β-to-α TCP transformation but also because of the lower mechanical properties of α-TCP compared to β-TCP.

In samples composited with Y_2O_3, the maximum $\sigma_{compressive}$ values of 258 ± 37.95, 227.75 ± 27.87, and 221.5 ± 28.04 MPa were obtained with increasing Y_2O_3

before β-to-α TCP transformation. These high $\sigma_{compressive}$ values for samples composited with Y_2O_3 were related to the fact that the amount of TCP phases was hindered by Y_2O_3 additives, which contributed to the formation of homogenous grains as well as high mechanical properties. As stated by Ref. [84], the ultimate $\sigma_{compressive}$ of human cortical bone ranges from 100 to 230 MPa. As can be seen from these values, although the HA-5A-0.5Y ternary composite had a higher $\sigma_{compressive}$ value compared to the human cortical bone, the others were in the range of $\sigma_{compressive}$ values of the human cortical bone.

The $\sigma_{T.P.B.}$ of pure HA changes between 33.9 and 112 MPa depending on the porosity ratio [85, 86]. The $\sigma_{T.P.B.}$ of pure HA used as a matrix material in the present study increased with increasing temperature and reached the maximum value of 60.27 ± 9.93 MPa at 1100 ºC. The maximum $\sigma_{T.P.B.}$ of pure HA decreased with increasing sintering temperatures as in the measurements of fracture toughness and compressive strength. The $\sigma_{T.P.B.}$ of the HA-5A composite without Y_2O_3 additive presented the maximum value of 75.70 ± 2.40 MPa at a temperature of 1200 ºC. An increment ratio of 25.6% was achieved compared to pure HA. With increasing sintering temperatures, as in the HA-5A composite, the $\sigma_{T.P.B.}$ values of Y_2O_3-added samples at amounts of 0.5 and 2.5 increased from 23.97 ± 5.11 MPa to 82.22 ± 8.45 MPa and from 31.05 ± 7.54 MPa to 84.87 ± 11.71 MPa, respectively. For HA-5A-1.5Y ternary composite, the $\sigma_{T.P.B.}$ value increased from 33.42 ± 7.47 MPa to 90.15 ± 6.93 MPa until the sintering temperature of 1200 ºC but decreased to 83.97 ± 11.89 MPa at 1300 ºC. It was also found that the $\sigma_{T.P.B.}$ of HA-5A (37.07 ± 10.62 MPa) sintered at 1300 ºC could be increased by Y_2O_3 additives at about 21.78%, 26.50%, and 28.92%. These values agreed with the $\sigma_{T.P.B.}$ value of the cortical bone which ranged from 50 to 150 MPa [87].

In vitro bioactivity properties

Due to it is necessary long period times, efforts, and high cost for in vivo testing [88], the in vitro test has been used to investigate the bioactivity property of a biomaterial, which will be placed in to human body. By in vitro testing, some properties of a biomaterial such as osteoclast activity and osteoblast activity can be analyzed using SEM [89, 90]. HA is a material that it has the more bioactivity compared to polymeric and metallic biomaterials. Moreover, there are also some problems about the utilization of polymeric and metallic materials in human body as following.

The resorbability rate of some polymeric materials are not compatible with the regeneration time of damaged tissues.

Polymeric materials may have toxic effects due to their low molecular weight as well as their non-polymerizable monomers, the materials required to start polymerization, various additives and catalysts.

In the case of corrosion and/or wear of a metallic biomaterial such as cobalt-chromium alloys or titanium alloys, they can be caused the lung diseases, painful muscle spasms, shortness of breath, failure to perform motor tasks, failure to perform cognitive functions, memory loss, severe headache, and loss of appetite [91, 92].

In the present study, the in vitro bioactivity tests were performed to the samples exhibiting the highest mechanical properties, during immersion times of 3, 7, 15, and 30 d. Fig. 16 shows the surface morphologies of pure HA sintered at 1100 ºC, as well as HA-5A and HA-5A-1.5Y composites sintered at 1200 ºC, respectively. Apatite crystals on the surface of the samples started to form at the end of a short immersion period like 3 d. The amount of apatite crystals, however, was higher than that of the composites. Moreover, compared with the HA-5A binary composite, the Y_2O_3 additive increased the amount of apatite layers. The addition of Y_2O_3 also caused a similar effect as reported previously [93]. After 7 d of immersing into the SBF solution, apatite crystals began to grow in a dendritic form instead of a cubic shape for pure HA. However, it continued to grow in cubic shapes for the composites. Large parts of the surface of the samples were covered by apatite layers after immersion time of 15 d. The apatites on the surface of pure HA and HA-5A-1.5Y composite, however, were thicker than that of HA-5A composite. All of the surfaces of the sintered samples immersed into the SBF solutions were covered by apatite layers after 30 d. It was determined that both morphologies and the amount of apatite layers deposited on the surface of the samples were different depending on the immersion time and compositions of the samples. These differences are due to the differences in porosity rates of the samples, the bioactivity properties of additive powders, and the type of interphases that occurred during sintering. The amount and proportion of the apatite layers formed on the surfaces of the samples held in the SBF solution increased as the porosity ratio increased [94]. The porosity ratios of the samples before immersing to the SBF solution were 26%, 3.32%, and 4.21% for monolithic HA, HA-5A, and HA-5A-1.5Y, respectively. Apatite formation followed the order of pure HA > HA-5A-1.5Y > HA-5A. Although Al_2O_3 has higher mechanical properties compared to the HA, it is well known that Al_2O_3 is a bioinert ceramic, so the addition of Al_2O_3 to HA reduces the bioactivity property of HA. Therefore, the in vitro bioactivity of HA-5A composite was lower than that of monolithic HA and HA-5A-1.5Y composite. It can be also said that HA-5A-1.5Y composite sintered at 1200 ºC can be used as a bone grafting material in human femur bone due to it has enough physical and mechanical strength values and invitro bioactivity property.

Conclusions

The mechanical properties of the sintered samples reached the maximum values just before densification was completed. At the maximum shrinkage rate of 18%, the densification rates of about 90% were obtained for HA samples with additives, and it was above 90% for monolithic HA. Although monolithic HA was stable until 1200 °C, additives of Al_2O_3 and Y_2O_3 reduced the decomposition temperature from 1200 °C to 900 °C. The decomposition rate of Al_2O_3-added samples without Y_2O_3 was higher than those of monolithic HA and HA-5A-Y ternary composites. It can be hindered by the addition of the Y_2O_3 powder at almost all sintering temperatures. Monolithic HA sintered at 1200 °C and 1300 °C exhibited an excessive grain growth and also microcracks which were minimized by the additives. The highest mechanical properties of monolithic HA could be improved by the additives. Although the addition of Al_2O_3 reduced the in vitro bioactivity of HA, the addition of Y_2O_3 to the HA-A composite improved the bioactivity. The optimum results in the HA-5A-Y ternary composite were obtained by adding 1.5% of Y_2O_3 powder. Because of the sufficient mechanical and in vitro bioactivity properties, the HA-5A-1.5Y composite sintered at 1200 °C can be potentially used in the human body.

Acknowledgements

This study was economically supported by Scientific Research Centre of Marmara University (Project No: FEN-A-100616-0272).

References

1. A. Pal, S. Paul, A.R. Choudhury, V.K. Balla, M. Das, A. Sinha, Mater. Lett. 203 (2017) 89-92.
2. M. Aminzare, A. Eskandari, M.H. Baroonian, A. Berenov, Z. Razavi Hesabi, M. Taheri, S.K. Sadrnezhaad, Ceram. Inter. 39 (2013) 2197-2206.
3. S. Lala, T.N. Maity, M. Singha, K. Biswas, S.K. Pradhan, Ceram. Inter. 43 (2017) 2389-2397.
4. N.J. Lóh, L. Simão, J. Jiusti, A. De Noni Jr., O.R.K. Montedo, Ceram. Inter. 43 (2017) 8269-8275.
5. M. Bahraminasab, S. Ghaffari, H. Eslami-Shahed, J. Mech. Behav. Biomed. Mater. 72 (2017) 82-89.
6. A. Yelten, S. Yilmaz, F.N. Oktar, Ceram. Inter. 38 (2012) 2659-2665.
7. S.J. Kim, H.G. Bang, J.H. Song, S.Y. Park, Ceram. Inter. 35 (2009) 1647-1650.
8. M.S. Hejazi, M. Ahmadian, M. Meratian, M.H. Fath, J. Mech. Behav. Biomed. Mater. 40 (2014) 95-101.
9. M. Rouahi, E. Champion, O. Gallet, A. Jada, K. Anselme, Colloids Surf. B 47 (2006) 10-19.
10. X. Guo, J.E. Gough, P. Xiao, J. Liu, Z. Shen, J. Biomed. Mater. Res. A 82[4] (2007) 1022-1032.
11. F.H. Lin, C.J. Liao, K.S. Chen, J.S. Sun, C.P. Lin, Biomaterials 22 (2001) 2981-2992.
12. M. Kon, K. Ishikawa, Y. Miyamoto, K. Asaoka, Biomaterials 16 (1995) 709-714.
13. A. Ślósarczyk, J. Piekarczyk, Ceram. Inter. 25 (1999) 561-565.
14. Z. Evis, A. Tahmasebifar, J. Ceram. Process. Res. 14 (2013) 549-556.
15. W. Suchanek, M. Yashima, M. Kakihana, M. Yoshimura, Biomaterials 18 (1997) 923-933.
16. Z. Evis, R.H. Doremus, Mater. Res. Bull. 43 (2008) 2643-2651.
17. L. Letue, J. Petit, M.H. Ritti, S. Lalanne, S. Landais, Mater. Chem. Phys. 194 (2017) 302-307.
18. A. Nakahira, K. Shiba, S. Yamaguchi, K. Kijima, Key Eng. Mater. 161-163 (1999) 177-180.
19. M. Sato, M.A. Sambito, A. Aslani, N.M. Kalkhoran, E.B. Slamovich, T.J. Webster, Biomaterials 27 (2006) 2358-2369.
20. K.E. Öksüz, A. Özer, Dig. J. Nanomater. Biostruct. 11[1] (2016) 167-172.
21. Designation: F 1185-88, American Society for Testing and Materials (ASTM), 1988
22. British Standart Non-Metallic Materials for Surgical Implants. Part 2: Specifications for Ceramic Materials Based on Alumina, BS 7253: Part 2: 1990 ISO 6474-1981
23. J. Majling, P. Znáik, A. Palová, S. Stevĭk, S. Kovalĭk, D.K. Agrawal, R. Roy, J. Mater. Res. 12[1] (1997) 198-202.
24. M. Rahimiana, N. Ehsani, N. Parvin, H. reza Baharvandi, J. Mater. Process. Technol. 209 (2009) 5387-5393.
25. O. Yeheskel, O. Tevet, J. Am. Ceram. Soc. 82[1] (1999) 136-144.
26. K. Niihara, J. Ceram. Soc. Jpn. 20 (1985) 12-18.
27. Standard Test Method for Flexural Strength of Advanced Ceramics at Ambient Temperature, Annual Book of ASTM standards, (1996)
28. T. Kokubo, T. Yamamuro, L.L. Hench, J. Wilson, (CRC Press, 1990) p.
29. J. Zhang, H. Tanaka, F. Ye, D. Jiang, M. Iwasa, Mater. Chem. Phys. 101 (2007) 69-76.
30. W. Liu, J. Chang, J. Biomater. Appl. 27[2] (2011) 171-178.
31. R.N. Palchesko, K.A. McGowan, E.S. Gawalt, Mater. Sci. Eng. C. 31 (2011) 637-642.
32. P.N. Kumar, J.M.F. Ferreira, S. Kannan, J. Eur. Ceram. Soc. 37 (2017) 2953-2963.
33. J.M.R. Mercury, A.H. de Aza, P. Pena, J. Eur. Ceram. Soc. 25 (2005) 3269-3279.
34. S. Barzilai, M. Aizenshtein, N. Froumin, N. Frage, Mater. Sci. Eng. A 420 (2006) 291-295.
35. S. Kume, I. Yamada, K. Watari, K. Mitsuishi, J. Soc. Mater. Sci. Jpn. 57[6] (2008) 528-531.
36. J. Wojewoda-Budka, N. Sobczak, J. Morgiel, J. Microsc. 237[3] (2010) 253-257.
37. A. Richter, M. Göbbels, J. Phase Equilibria Diffus. 31 (2010) 157-163.
38. D.H. Kothari, D.K. Kanchan, Physica B. 501 (2016) 90-94.
39. G. Li, T. Long, Y. Song, G. Gao, J. Xu, B. An, S. Gan, G. Hong, J. Rare Earth. 28[1] (2010) 22-25.
40. R.J. Wiglusz, T. Grzyb, A. Lukowiak, A. Bednarkiewicz, S. Lis, W. Strek, J. Lumin. 133 (2013) 102-109.
41. W.W. Rudolph, G. Irme, Dalton Trans. 44 (2015) 18492-18505.
42. E.I. Suvorova, V.V. Klechkovskaya, V.F. Komarov, A.V. Severin, I.V. Melikhov, P.A. Buffat, Crystallogr. Rep. 51[5] (2006) 881-887.
43. Z. Evis, J. Ceram. Soc. Jpn. 114[11] (2006) 1001-1004.
44. M.A. Lopes, J.D. Santos, F.J. Monteiro, J.C. Knowles, J.

Biomed. Mater. Res. 39[2] (1998) 244-251.
45. I. Manjubala, T.S.S. Kumar, Biomaterials. 21 (2000) 1995-2002.
46. H.W. Kim, Y.J. Noh, Y.H. Koh, H.E. Kim, J. Mater. Sci. Mater. Med. 14 (2003) 899-904.
47. M.A. Lopes, F.J. Monteiro, J.D. Santos, Biomaterials. 20 (1999) 2085-2090.
48. A. Ślósarczyk, M. Klisch, M. Błaẑewicz, J. Piekarczyk, L. Stobierski, A. Rapacz-Kmita, J. Eur. Ceram. Soc. 20 (2000) 1397-1402.
49. H. Xu, H. Guo, Thermal Barrier Coatings, Wood Head Publishing, Cambridge, UK, 2011.
50. https://www.osti.gov/scitech/biblio/4840970
51. E. Harabi, A. Harabi, L. Foughali, S. Chehlatt, S. Zouai, F.Z. Mezahi, Acta Phys. Pol., A 127[4] (2015) 1161-1163.
52. S.F. Mansour, S.I. El-dek, M.K. Ahmed, Sci. Rep. 7 (2017) 43202.
53. D.S. Seo, J.K. Lee, Met. Mater. Int. 15[2] (2009) 265-271.
54. P. Layrolle, A. Ito, T. Tateishi, J. Am. Ceram. Soc. 81[6] (1998) 1421-1428.
55. I.R. Gibson, S.M. Best, W. Bonfield, J. Am. Ceram. Soc. 85[11] (2002) 2771-2777.
56. L.G. Teoh, J. Shieh, W.H. Lai, M.H. Hon, J. Mater. Res. 19[9] (2004) 2687-2693.
57. S. Khoshsima, B. Yilmaz, A. Tezcaner, Z. Evis, Ceram. Inter. 42 (2016) 15773-15779.
58. Z. Evis, M. Usta, I. Kutbay, Mater. Chem. Phys. 110 (2008) 68-75.
59. S. Griza, D.H.G. de Souza Sá, W.W. Batista, J.C.G. de Blas, L.C. Pereira, Mater. Des. 56 (2014) 200-208.
60. A. Mahapatro, Mater. Sci. Eng. C. 55 (2015) 227-251.
61. V.V. Silva, F.S. Lameiras, R.Z. Domingues, Compos. Sci. Technol. 61 (2001) 301-310.
62. M. Ashok, N.M. Sundaram, S.N. Kalkura, Mater. Lett. 57 (2003) 2066-2070.
63. H.W. Kim, Y.M. Kong, Y.H. Koh, H.E. Kim, H.M. Kim, J.S. Ko, J. Am. Ceram. Soc. 86[12] (2003) 2019-2026.
64. Y.W. Gu, N.H. Loh, K.A. Khor, S.B. Tor, P. Cheang, Biomaterials. 23 (2002) 37-43.
65. K.A. Khalil, S.W. Kim, H.Y. Kim, Mater. Sci. Eng. A 456 (2007) 368-372.
66. Y.W. Gu, K.A. Khor, P. Cheang, Biomaterials. 25 (2004) 4127-4134.
67. R. Kumar, P. Cheang, K.A. Khor, J. Mater. Process. Technol. 140 (2003) 420-425.
68. V.P. Orlovskii, V.S. Komlev, S.M. Barinov, Inorg. Mater. 38[10] (2002) 973-984.
69. I.H. Arita, D.S. Wilkinson, M.A. Mondragón, V.M. Castaño, Biomaterials. 16 (1995) 403-408.
70. S. Bose, S. Dasgupta, S. Tarafder, A. Bandyopadhyay, Acta Biomater. 6 (2010) 3782-3790.
71. D. Veljović, G. Vuković, I. Steins, E. Palcevskis, P.S. Uskoković, R. Petrović, D. Janaćković, Sci. Sinter. 45 (2013) 233-243.
72. S. Kim, Y.M. Kong, I.S. Lee, H.E. Kim, J. Mater. Sci. Mater. Med. 13 (2002) 307-310.
73. S. Gautier, E. Champion, D. Bernache-Assollant, J. Mater. Sci. Mater. Med. 10 (1999) 533-540.
74. S.P. Khanal, H. Mahfuz, A.J. Rondinone, T.H. Leventouri, Mater. Sci. Eng. C 60 (2016) 204-210.
75. A.J. Ruys, M. Wei, C.C. Sorrell, M.R. Dickson, A. Brandwood, and B.K. Milthome Biomaterials. 16 (1995) 409-415.
76. T. Matsuno, K. Watanabe, K. Ono, M. Koishi, J. Mater. Sci. Lett. 19 (2000) 573-576.
77. N.R. Patel, P.P. Gohil, Int. J. Emerging Technol. Adv. Eng. 2[4] (2012) 91-101.
78. H.W. Kim, Y.J. Noh, Y.H. Koh, H.E. Kim, J. Mater. Sci. Mater. Med. 14 (2003) 899-904.
79. S. Tayebi, F. Mirjalili, H. Samadi, A. Nemati, J. Ceram. Process. Res. 17[10] (2016) 1033-1041.
80. S.J. Kalita, H.A. Bhatt, A. Dhamne, J. Am. Ceram. Soc. 89[3] (2006) 875-881.
81. A. Bandyopadhyay, S. Bernard, W. Xue, S. Bose, J. Am. Ceram. Soc. 89[9] (2006) 2675-2688.
82. R.G. Carrodeguas, S.D. Aza, Acta Biomater. 7 (2011) 3536-3546.
83. S. Wang, Y. Wang, K. Sun, X. Sun, Process. App. Ceramics 11[2] (2017) 100-105.
84. V.V. Silva, F.S. Lameiras, R.Z. Domingues, Compos. Sci. Technol. 61 (2001) 301-310.
85. H.Y. Yasuda, S. Mahara, N. Terashita, Y. Umakoshi, Mater. Trans. 43[6] (2002) 1332-1335.
86. R. Chumnanklang, T. Panyathanmaporn, K. Sitthiseripratip, J. Suwanprateeb, Mater. Sci. Eng. C 27 (2007) 914-921.
87. K. Takahashi, Y. Fujishiro, S. Yin, T. Sato, Ceram. Inter. 30 (2004) 199-203.
88. M.A. Lopes, J.C. Knowles, J.D. Santos, F.J. Monteiro, I. Olsen, Biomaterials. 21 (2000) 1165-1172.
89. S. Langstaff, M. Sayer, T.J.N. Smith, S.M. Pugh, S.A.M. Hesp, W.T. Thompson, Biomaterials. 20 (1999) 1727-1741.
90. J.D. Santos, R.L. Reis, F.J. Monteiro, J. Mater. Sci. Mater. Med. 6 (1995) 348-352.
91. A.K. Bajpai, J. Bajpai, R.K. Saini, P. Agrawal, A. Tiwari, Smart Biomaterial Devices Polymers in Biomedical Sciences, CRC Press, Taylor & Francis Group, LLC, Abingdon, U.K. (2017)
92. S. Suzuki, Y. Ikada, Biomaterials for Surgical Operation. Springer Science+Business Media, LLC, New York, USA. (2012)
93. D. Cacaina, H. Ylänen, M. Hupa, S. Simon, J. Mater. Sci. Mater. Med. 17 (2006) 709-716.
94. Q.Z. Chen, K. Rezwan, D. Armitage, S.N. Nazhat, A.R. Boccaccini, J. Mater. Sci. Mater. Med. 17 (2006) 979-987.